String operators for Cheshire strings in topological phases

Nathanan Tantivasadakarn [1] and Xie Chen [1,2]
[1] *Walter Burke Institute for Theoretical Physics and Department of Physics, California Institute of Technology, Pasadena, California 91125, USA*
[2] *Institute for Quantum Information and Matter, California Institute of Technology, Pasadena, California 91125, USA*

(Received 2 December 2023; revised 23 March 2024; accepted 12 April 2024; published 25 April 2024)

Elementary point charge excitations in three-plus-one-dimensional (3+1D) topological phases can condense along a line and form a descendant excitation called the Cheshire string. Unlike the elementary flux loop excitations in the system, Cheshire strings do not have to appear as the boundary of a 2D disk and can exist on open line segments. On the other hand, Cheshire strings are different from trivial excitations that can be created with local unitaries in zero dimensions and finite depth quantum circuits in one dimension and higher. In this paper, we show that to create a Cheshire string, one needs a linear depth circuit that acts sequentially along the length of the string. Once a Cheshire string is created, its deformation, movement and fusion can be realized by finite depths circuits. This circuit depth requirement applies to all nontrivial descendant excitations including symmetry-protected topological chains and the Majorana chain.

DOI: 10.1103/PhysRevB.109.165149

I. INTRODUCTION

Cheshire strings describe linelike excitations in topological states, which contain a mysterious hidden charge along the length of the string [1,2]. The charge content cannot be pinpointed to one or a few local regions on the string and therefore costs no extra energy compared to the zero charge state. The degeneracy is a result of the spontaneous symmetry breaking, or more precisely Higgsing, of (part of) the gauge symmetry in the topological phase and the condensation of the corresponding gauge charges along the string. Since the gauge charge is condensed, adding more does not change the energy of the condensate.

Cheshire strings have been included as an essential part in the formulation of a complete mathematical description of three-plus-one-dimensional (3 + 1D) topological orders in terms of higher categories [3–13]. In Ref. [5], the example of 3 + 1D toric code was discussed explicitly where fundamental objects in the higher category include 1D objects such as the Cheshire string and magnetic gauge flux loop and the 0D domain walls between them, which includes the electric gauge charge excitation. From a physics perspective, it is not immediately clear why a consistent theory of the 3 + 1D $\mathbb{Z}_2$ topological order needs to involve the Cheshire string. After all, the elementary excitations—the gauge charge and gauge flux—capture all the fractional statistics we see in the model and their corresponding string and membrane operators capture the full logical operations in the degenerate ground space. The Cheshire string is made of gauge charges and in this sense a descendant excitation [6]. Are they really necessary in the description?

Some observations point to the intrinsic nature of Cheshire strings in 3 + 1D topological phases. First of all, they do exist as a 1D excitation in the model and can hence appear next to magnetic flux loops and change their feature. In non-Abelian gauge theories, it has long been known that magnetic flux loops are intrinsically Cheshire as the flux loop breaks the non-Abelian gauge symmetry down to a subgroups and therefore gauge charges that transform nontrivially under the broken part of the gauge group have to condense along the loop [1,2]. In Abelian gauge theories with nontrivial three-loop braiding [14–21], some flux loops are intrinsically Cheshire as well. Such flux loops can be thought of as the boundary between different 2 + 1D gauge theories and can only be gapped if the gauge charge is condensed along the loop [5].

The following questions and answers may help clarify the situation.

(1) Do we need to include Cheshire points in our description of topological order as well?

We already have. A Cheshire point can be obtained by shrinking the Cheshire string to a point and is a direct sum of all charge states. In the $\mathbb{Z}_2$ case, it is $1 \oplus e$. When the condensate is zero dimensions, the degeneracy between the two charge states will generically split and we end up with either 1 or e.

(2) Why did we not include Cheshire strings in the description of 2 + 1D topological order?

2 + 1D topological orders are characterized in terms of braided fusion categories whose fundamental objects are point excitations—the anyons. Cheshire strings appear at one higher dimension and hence do not mix with the anyons. However, they do play an important role as defects and boundaries of the topological states and are described as (bi)module categories over the bulk fusion category, as explained in Ref. [22].

(3) Apart from Cheshire strings, are there other types of descendant excitations?

Yes. Cheshire strings correspond to the 1 + 1D symmetry-breaking phase of the gauge charge. There are also invertible phases such as symmetry-protected topological phases in 1 + 1D. For example, when the gauge charge is a fermion, there is also the Majorana chain. Cheshire strings are a noninvertible

excitations while the latter two correspond to invertible descendant excitations. (References [23–27] construct examples of such excitations.) Going to higher dimensions, we would also need to consider membranelike descendant excitations of point and loop excitations.

(4) What is the benefit of including Cheshire string in the description of topological orders?

One benefit is that it makes the correspondence between bulk and boundary more natural (at least in a mathematical sense as shown in Refs. [9,22,28,29]).

(5) The elementary excitations are generated with unitary string and membrane operators. Does this also apply to Cheshire string?

Yes, this is what we are going to show in this paper. Previous discussions have mostly focused on generating Cheshire string by changing the Hamiltonian of the topological state or using projection operations [5]. We want to emphasize that Cheshire strings can also be generated using unitary circuits and the way it is generated using unitary circuits makes clear its nontrivialness as a descendant excitation. Magnetic fluxes are nontrivial loop excitations because they can only be generated as the boundary of a unitary membrane operator. Because of that, they have to form closed loops. Cheshire strings, on the other hand, do not have to appear on the boundary of a membrane and can exist on open string segments (i.e., they admit a topological boundary). However, if we would like to generate a Cheshire string with a unitary circuit along the string, the circuit depth has to grow linearly with the length of the string.[1] The linear depth of the circuit distinguishes Cheshire strings from trivial linelike excitations that can be generated with finite depth circuits. In particular, as we show below, the linear depth circuit has a sequential structure. That is, each layer contains only one local gate set acting on a local region in the string. The gate set moves from one end point of the string to the other and acts on the string in sequential way. This is hence an example of a sequential quantum circuit [30–34]. Once a Cheshire string has been created, we show that it can be deformed, moved, and fused using finite depth circuits. Therefore, the equivalence relation between Cheshire excitations can be established with finite depth circuits, similar to the case of elementary point and loop excitations.[2]

The paper is structured as follows. In Sec. II, we show how to generate a Cheshire string in $2+1$D toric code using a sequential linear depth circuit. In Sec. III, we show how to deform, move, and fuse Cheshire strings in $2+1$D toric code. In Sec. IV, we show how similar circuits work in $(3+1)$

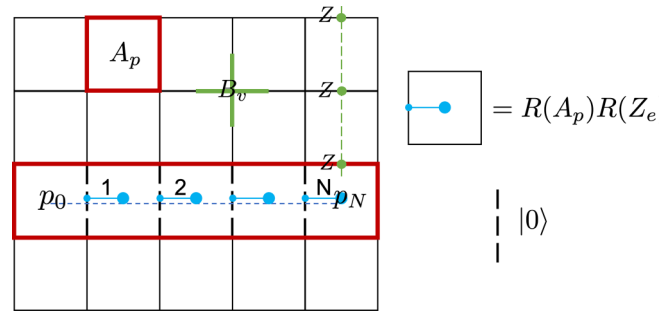

FIG. 1. Generation of an e-Cheshire string in $2+1$D toric code with a sequential circuit. A_p and B_v are Hamiltonian terms of the $2+1$D toric code. A Cheshire string (on the dual lattice) from p_0 to p_N is generated by applying a sequence of gate sets represented by the blue dot pairs. The dashed black edges are mapped to the product state $|0\rangle$ forming the condensate, while the total charge of the condensate measured by $\prod X$ around the red loop is conserved. Adding an e charge using the string of Z along the dashed green line maps between the two degenerate states of the condensate.

dimensions. In fact, in the $2+1$D toric code, there are five types of nontrivial defects [25,26]. Their creation and fusion can be achieved similarly with sequential linear depth circuits/finite depth circuits. We demonstrate this in Appendix A. In the summary section (Sec. V), we discuss the relation between different types of excitations in topological phases and the unitary operation that generates them.

II. GENERATION OF CHESHIRE STRING IN (2+1) DIMENSIONS

Let us first consider the generation of a Cheshire string in the $2+1$D toric code. Consider the toric code on two-dimensional lattice defined with the Hamiltonian

$$H = -\sum_p A_p - \sum_v B_v = -\sum_p \prod_{e\in p} X_e - \sum_v \prod_{v\in e} Z_e. \quad (1)$$

Let us call excitation of the A_p terms the gauge charge excitation labeled by e and the excitation of the B_v terms the gauge flux excitation labeled by m. Applying Z_e on one edge creates two gauge charge excitations on the neighboring plaquettes. Having a charge condensate corresponds to enforcing $-Z_e$ as the Hamiltonian term so that the ground state remains invariant under the pair creation or hopping of gauge charges between the neighboring plaquettes. If such a term is enforced on a string of edges on the dual lattice (dotted blue line in Fig. 1), we get a Cheshire string for the gauge charge e.

While the Cheshire string can be generated with projection operators $\frac{1}{2}(1+Z_e)$ acting on the edges along the string all at the same time, generating it with unitary operations takes a number of steps that scales linearly with the length of the string. Consider creating a Cheshire string on the dual lattice, which starts at a plaquette p_0 and ends at plaquette p_N, adjacent plaquettes in the sequence p_i and p_{i+1} share an edge $e_{i,i+1}$. The sequential circuit to create the Cheshire charge is

[1] An argument is the following: suppose there exists a finite depth circuit to create a Cheshire string, we may use it to create two Cheshire strings of extensive length and extensive separation in the system size. This configuration now has an additional ground-state degeneracy. The degeneracy can be labeled by the amount of charge on each Cheshire string, which can only be detected nonlocally by moving a flux around one of the Cheshire strings. Moreover, changing the amount of charge on each Cheshire string requires an operator of extensive support, which is the string operator of the charge. Since this degeneracy is robust, it is a contradiction.

[2] Equivalence relations between point excitations are given by local unitary transformations.

given by

$$U = \prod_{i=N}^{1} R(A_{p_i}) R(Z_{e_{i-1,i}}), \tag{2}$$

where we define $R(\mathcal{O}) \equiv e^{-\frac{i\pi}{4}\mathcal{O}}$, which has the property that for Pauli operators P and Q,

$$R(Q)PR(Q)^\dagger = \begin{cases} P; & [P,Q]=0 \\ iPQ; & \{P,Q\}=0 \end{cases}. \tag{3}$$

Note that the R gates do not commute with each other so the ordering is important. Our convention is that gates to the right are applied before gates to the left. Therefore, the sequence of gates are $R(Z_{e_{0,1}})$, $R(A_{p_1})$, $R(Z_{e_{1,2}})$, $R(A_{p_2})$, and so forth. Since A_p and Z_e commutes with the vertex term, the circuit leaves the vertex stabilizers invariant while mapping

$$\begin{aligned} A_{p_i} &\to Z_{e_{i-1,i}}, \quad i = 1, \ldots, N \\ A_{p_0} &\to \prod_{i=0}^{N} A_{p_i} \prod_{i=1}^{N} Z_{e_{i-1,i}}. \end{aligned} \tag{4}$$

Therefore, after the circuit, the edges along the dual string are in the condensate state $|0\rangle$ stabilized by Z_e. The total charge of the condensate measured by $\prod_{i=0}^{N} A_{p_i}$ remains invariant in the ground state, while the individual charges A_{p_i} are no longer conserved. Adding an e charge using the string of Z operators along the dashed green line changes the total charge of the condensate, but does not affect the local terms in the condensate. Therefore, the two total charge states are degenerate on the Cheshire string.

Generating a Cheshire string—a condensate for the gauge charge e—in the toric code corresponds to opening up a slit of vacuum state inside the topological bulk with a smooth boundary between the two. Similar operations (or the inverse) have been discussed in Refs. [35–37]. In Appendix A, we are going to discuss how a similar condensate of the gauge flux m corresponds to a rough boundary between toric code and the vacuum.

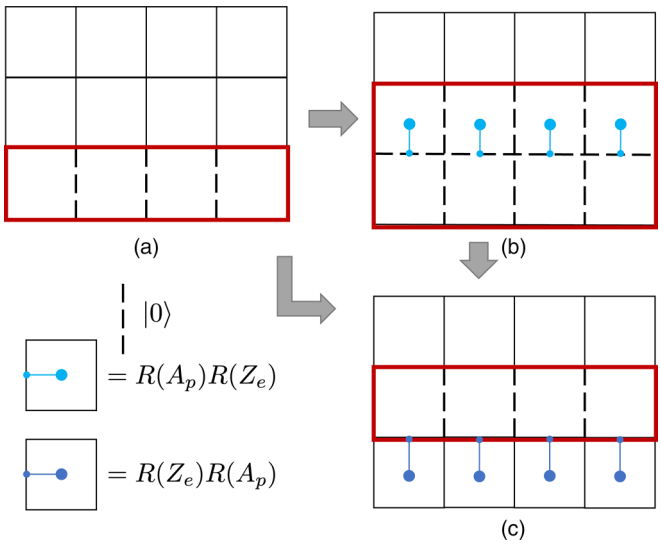

FIG. 2. Deforming [(a) to (b) and (b) to (c)] and moving [(a) to (c)] a Cheshire string using finite depth circuit in $(2+1)$ dimensions. The gate sets in each diagram can be applied in parallel. The dashed black edges are in the $|0\rangle$ state of the condensate. Red loop of $\prod X$ measures the total charge in the condensate.

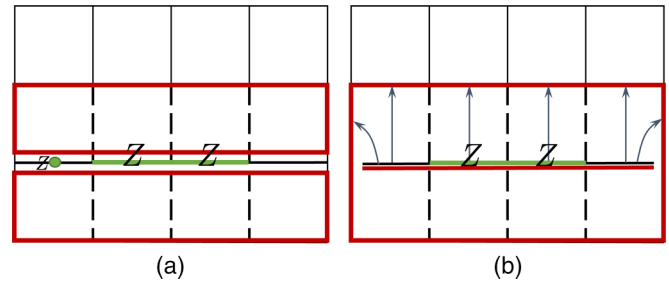

FIG. 3. Fusion of two Cheshire strings with a finite depth circuit in $(2+1)$ dimensions. (a) Before fusion, $\prod X$ around each red rectangle measures the total charge on each string. Qubits on the domain wall are coupled with ZZ terms (green bond). A single Z on the domain wall (green dot) tunnels a charge between the two condensates. (b) Applying the controlled-NOT gates indicated by the arrows, the domain wall qubits are decoupled from the bulk. The ZZ coupling remains, giving rise to twofold degeneracy.

III. FUSION OF CHESHIRE STRING IN (2+1) DIMENSIONS

Once a Cheshire string is created, it can be deformed, moved, and fused using finite depth circuits. In other words, finite depth circuits establish the equivalence relation between Cheshire string excitations.

As shown in Fig. 2, if we start from a Cheshire string in the bottom row [Fig. 2(a) with dashed black edges in state $|0\rangle$], we can make it thicker [Fig. 2(b)] and then thinner [Fig. 2(c)] using finite depth circuits. The individual gate sets (the blue dot pairs) take the same (inverse) form as in Fig. 1. The difference is that now the gate sets are oriented in parallel, rather than connecting head to toe. It can be easily checked that parallel gate sets commute with each other and hence can be applied simultaneously. Going from Figs. 2(a) to 2(c) moves the Cheshire string perpendicular to its length by one step. The total charge of the condensate, measured by $\prod X$ along the red loop, is conserved in the whole process.

Two identical Cheshire strings c defined on a segment fuse as[3]

$$c \times c = 2c, \tag{5}$$

which can be realized with finite depth circuit as well. Using the circuits discussed above, we can always move the two strings with finite separation right next to each other as shown in Fig. 3(a) with a finite depth circuit.

[3]More generally, the coefficient of the fusion depends on the space-time manifold of the string [25]. Explicitly, for a Cheshire string supported on a spatial manifold M, the coefficient is the partition function of a 1+1D $\mathbb{Z}_2$ gauge theory on $M \times S^1$, i.e., it is the degeneracy of a 1+1D $\mathbb{Z}_2$ ferromagnet on M.

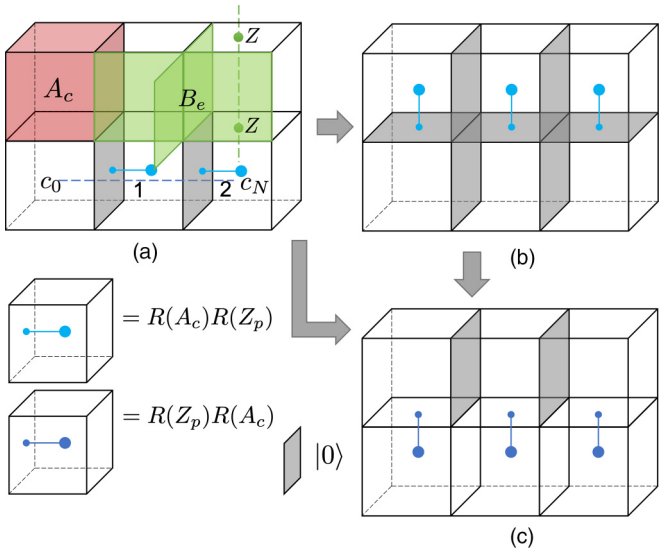

FIG. 4. Creating, deforming and moving Cheshire string in 3 + 1D toric code. A_c and B_e are Hamiltonian terms in the toric code. (a) Cheshire string along the dual string (blue dotted line) can be generated with a sequential circuit along the length of the string. Once the string is created, it can be deformed [(a) to (b) and (c) to (d)] and moved [(a) to (c)] with finite depth circuits.

Before fusing, $\prod X$ around the red rectangles measures the charge on each string. Along the domain wall separating the two strings, the Hamiltonian involves pairwise ZZ terms as shown by the green bond in Fig. 3(a). A single Z on the domain wall tunnels a charge from one string to another. It spoils the conservation of charge on each string while preserving their sum.

The fusion of the strings can be achieved with the finite depth circuit shown in Fig. 3(b). Each arrow represents a controlled-NOT gate with the start of the arrow being the control and the end of the arrow being the target. All the gates commute and can be applied in one step. After the circuit, the domain wall separating the two strings become completely decoupled from topological bulk. The ZZ couplings along the domain wall remain invariant, resulting in a twofold degeneracy between the $|00\ldots0\rangle$ state and the $|11\ldots1\rangle$ state. When the domain wall is in the $|00\ldots0\rangle$ state, it merges naturally with the condensates on the two sides into a single condensate. When the domain wall is in the $|11\ldots1\rangle$ state, a simple one-step rotation would take it into the $|00\ldots0\rangle$ state and the same conclusion holds. Therefore, two Cheshire strings merge into one Cheshire string with a prefactor of 2. If one wants to put the fused string into a standard form (e.g., of width 1), this can be done with another finite depth circuit of the form in Fig. 2(c).

IV. CHESHIRE STRING IN (3+1) DIMENSIONS

A similar construction holds in 3 + 1D toric code as well. Consider the 3 + 1D toric code on a cubic lattice with Z_2 qubits on the plaquettes. The Hamiltonian contains a charge term A_c around each cube c and a flux term B_e around each edge e, as shown in Fig. 4(a).

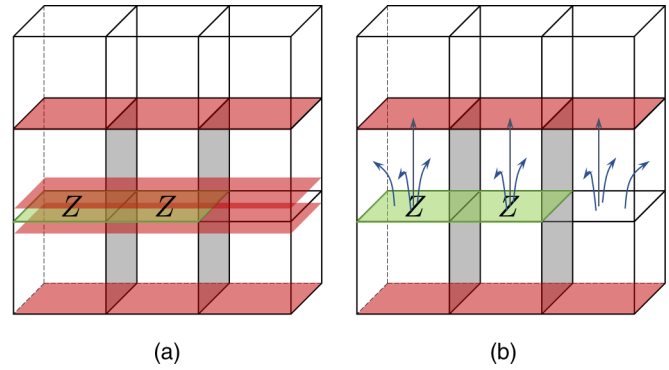

FIG. 5. Fusion of two Cheshire strings with a finite depth circuit in (3 + 1) dimensions. (a) Before fusion, $\prod X$ around each red rectangular cuboid measures the total charge on each string. The front and back faces of the cuboid are not shaded red for clarity. Qubits on the domain wall are coupled with ZZ terms (the green plaquette pair). (b) Applying the controlled-NOT gates indicated by the arrows, the domain wall qubits are decoupled from the bulk. The ZZ coupling remains, giving rise to the twofold degeneracy.

$$H = -\sum_c A_c - \sum_v B_v$$
$$= -\sum_c \prod_{p\in c} X_p - \sum_e \prod_{e\in p} Z_p. \tag{6}$$

Similar to the 2 + 1D case, applying Z_p on one plaquette creates two gauge charge excitations in the neighboring cubes. A Cheshire string corresponds to enforcing $-Z_p$ on the plaquettes along a dual string [the dotted blue line in Fig. 4(a)].

As shown in Fig. 4(a), a Cheshire string from cube c_0 to c_N can be created with a sequential circuit

$$U = \prod_{i=N}^{1} R(A_{c_i})R(Z_{p_{i-1,i}}). \tag{7}$$

The circuit leaves the B_e terms invariant while mapping

$$A_{c_i} \to Z_{p_{i-1,i}}, \quad i = 1, \ldots, N$$
$$A_{c_0} \to \prod_{i=0}^{N} A_{c_i} \prod_{i=1}^{N} Z_{p_{i-1,i}}. \tag{8}$$

Similar to the 2 + 1D case, the shaded plaquettes are mapped to the $|0\rangle$ state of the condensate while the total charge of the condensate measured by $\prod_{i=0}^{N} A_{c_i}$ remains invariant in the ground state. Adding an e charge using the string of Z operators along the dashed green line maps between the two degenerate states of the Cheshire string. By generating a Cheshire string in the bulk of the toric code state, we create the vacuum state in a linelike region with a smooth gapped boundary to the topological bulk. Similar operations (or the inverse) have been discussed in Ref. [38].

Once a Cheshire string is created, it can be deformed [Figs. 4(a) to 4(b) or 4(b) to 4(c)] and moved [Figs. 4(a) to 4(c)] with finite depth circuits. Fusion of two Cheshire strings proceeds in a similar way as in (2 + 1) dimensions. As shown in Fig. 5(a), when two Cheshire strings (gray shaded

TABLE I. Generation and equivalence of excitations in topological states with unitaries. LU refers to local unitary; FD refers to finite depth circuit; SLD refers to sequential linear depth circuit. The top section is for elementary excitations and the bottom section is for descendant excitations.

Topological excitations	Generated by	Equivalence
Abelian anyon	FD 1D	LU
non-Abelian anyon	SLD 1D	LU
Abelian flux loop	FD 2D	FD 1D
non-Abelian flux loop	SLD 2D	FD 1D
invertible 1D descendant	FD 2D or SLD 1D	FD 1D
noninvert. 1D descendant	SLD 1D	FD 1D

plaquettes) lie next to each other, the plaquettes on the domain wall between them couple with ZZ terms. The operator $\prod X$ around each red rectangular cuboid measures the total charge on each string. (The front and back faces of the cuboid are not shaded red for clarity.) Applying the controlled-NOT gates indicated by the arrows in Fig. 5(b), the domain wall qubits are decoupled from the topological bulk. The ZZ coupling remains, giving rise to a twofold degeneracy of $|00\ldots0\rangle$ and $|11\ldots1\rangle$, each of which merges with the two condensates into one condensate.

V. SUMMARY

By discussing the generation and fusion of the Cheshire string using unitary circuits, we put it under the same framework as other excitations of a topological system. Table I summarizes the different cases. We expect that higher-dimensional descendant excitations can also be systematically generated by sequential circuits with linear depth in their corresponding dimensions.

Anyons in $(2+1)$ dimension and gauge charge/gauge flux excitations in $(3+1)$ dimensions are generated as the boundary of a higher-dimensional unitary operator. Anyons and gauge charges are generated as the end point of a string operator while gauge fluxes are generated as the boundary of a membrane operator. When the excitation is Abelian, the string/membrane operator can be implemented with a finite depth circuit. In other words, small pieces of the string/membrane operator can be connected without defect. When the excitation is non-Abelian, the string/membrane operator has to be implemented sequentially, and requires a sequential linear depth circuit in one/two dimensions. Such excitations are called elementary excitations.

Descendant excitations such as Cheshire string on the other hand do not have to be created as a closed loop and hence can live on open strings (or higher-dimensional discs). They are nontrivial in the sense that when they are created in the dimension they are in, a sequential linear depth circuit is needed while trivial excitations are created with finite depth circuits. Among the descendant excitations, some are invertible, such as SPT states and Majorana chains, etc. The invertible excitations can also be created as the boundary of a higher-dimensional unitary and in this case a finite depth circuit is enough. The noninvertible ones, on the other hand, cannot be created with finite depth circuit even as the boundary of one higher dimension.

Once the excitations are created, their equivalence is established by local unitary operations if the excitation is zero dimensions and by finite depth circuits of n dimensions if the excitation is n dimensions. That is, the excitations can be deformed, moved, and fused using such unitaries.

ACKNOWLEDGMENTS

We are indebted to inspiring discussions with L. Kong, J. McGreevy, and X.-G. Wen. X.C. is supported by the National Science Foundation under Award No. DMR-1654340, the Simons collaboration on "Ultra-Quantum Matter" (Grant No. 651438), the Simons Investigator Award (Award ID 828078) and the Institute for Quantum Information and Matter at Caltech. N.T. and X.C. are supported by the Walter Burke Institute for Theoretical Physics at Caltech.

APPENDIX A: OTHER TYPES OF DEFECTS IN 2+1D TORIC CODE

Following the notation in Ref. [25], the Cheshire string discussed in Secs. II and III is a defect of the $2+1$D toric code labeled by S_e. There are four more types of nontrivial defects in $2+1$D toric code—S_m, S_ψ, S_{em}, and S_{me}. Their generation and fusion follow very similar rules. To generate these nontrivial descendant defects on an open interval, a linear depth sequential circuit is needed. To deform, move or fuse these defect, a finite depth circuit is sufficient. In this section, we demonstrate explicitly the generation of S_m, S_ψ, and the fusion of $S_{em}\times S_e = S_e$, $S_\psi \times S_e = S_m$, and $S_\psi \times S_\psi = S_1$, where S_1 is the trivial defect. All other generation and fusion processes can be derived from here. For the fusion process, we will show how the circuit works in the bulk of the defect without involving the end points. The end points usually lead to extra complications but do not change the fusion result.

In all figures, dashed black edges are in the $|0\rangle$ state stabilized by Z and dash-dotted black edges are in the $|+\rangle$ state stabilized by X. No-arrow connectors represent the controlled-Z gate:

$$U_{CZ} = \begin{pmatrix} 1 & 0 & 0 & 0 \\ 0 & 1 & 0 & 0 \\ 0 & 0 & 1 & 0 \\ 0 & 0 & 0 & -1 \end{pmatrix}. \tag{A1}$$

One-arrow connectors represent the controlled-X gate with the arrow pointing to the target:

$$U_{CX} = \begin{pmatrix} 1 & 0 & 0 & 0 \\ 0 & 1 & 0 & 0 \\ 0 & 0 & 0 & 1 \\ 0 & 0 & 1 & 0 \end{pmatrix}. \tag{A2}$$

Two-arrow connectors represent the X-controlled-Not gate, which is the controlled-X gate with the control qubit

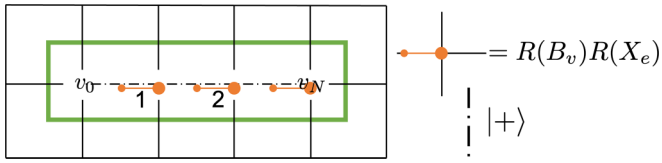

FIG. 6. Generation of S_m with a sequential linear depth circuit. The orange gate sets are applied sequentially from left to right. $\prod Z$ around the green box measures the total flux on S_m.

conjugated by the Hadamard gate:

$$U_{\mathrm{XCX}} = \frac{1}{2}\begin{pmatrix} 1 & 1 & 1 & -1 \\ 1 & 1 & -1 & 1 \\ 1 & -1 & 1 & 1 \\ -1 & 1 & 1 & 1 \end{pmatrix}. \tag{A3}$$

The gauge flux m is dual to the gauge charge e in toric code by switching between lattice and dual lattice and between X and Z operators. Therefore, to generate the S_m defect from vertex v_0 to vertex v_N, a sequential circuit of the form

$$U = \prod_{i=N}^{1} R(B_{v_i})R(X_{e_{i-1,i}}) \tag{A4}$$

as shown in Fig. 6 can be applied, where again $R(O) = e^{-i\frac{\pi}{4}O}$. This circuit maps B_{v_i} to $X_{e_{i-1,i}}$ while leaving all plaquette Hamiltonian terms invariant. It hence opens up a slit of vacuum state with a rough boundary to the topological bulk.

The S_ψ defect is an invertible domain wall inside the topological bulk, which permutes e and m excitations. That

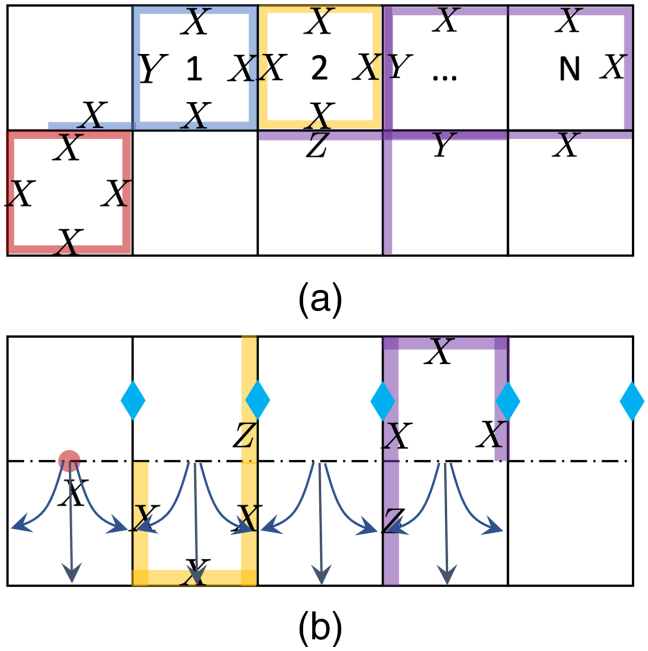

FIG. 7. Generation of S_ψ with a sequential linear depth circuit. The five-body blue term is used for the sequential part of the circuit. Following that there are two finite depth steps: the controlled-X gates represented by the arrows and the Hadamard gate represented by the blue diamonds. Hamiltonian terms before and after the circuit are shown with corresponding colors (red, yellow, and purple).

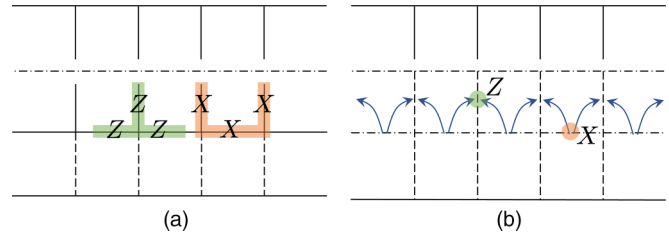

FIG. 8. Fusion of S_e [bottom in (a)] with S_m [top in (a)] into S_{em} [(b)] with a finite depth circuit. The circuit is composed of commuting controlled-Not gates represented by the arrows. All qubits on the domain wall between the two defects are decoupled after the circuit.

is, if an e excitation goes through the defect, it comes out as m and vice versa. The S_ψ defect can be generated with a sequential circuit as shown in Fig. 7. Denote the blue term in Fig. 7(a) around plaquette 1 as O_1. The first step of the circuit is

$$U = \prod_{i=N}^{1} R(O_i). \tag{A5}$$

This step is a sequential linear circuit. The second step is composed of controlled-X gates represented by the one-arrow connectors in the bottom plaquettes, as well as $R(Z)$s represented by blue diamonds, as shown in Fig. 7(b). The gates in the second step all commute with each other, therefore the second step has depth one. Hamiltonian terms before and after the circuit are shown with corresponding colors (red, yellow, and purple) in Figs. 7(a) and 7(b). The resulting terms take the same form as in Fig. 1 of Ref. [22]. A different version of the circuit was proposed in Ref. [39] and implemented in Ref. [40].

Figure 8 shows the fusion of S_e and S_m into S_{em}. In Fig. 8(a), the bottom defect is the S_e defect with smooth boundaries on the two sides and the top defect is the S_m defect with rough boundaries on the two sides. Applying the controlled-Not gates represented by the one-arrow connectors in Fig. 8(b) maps the three-body Hamiltonian terms on the domain wall between the two defects [shown in Fig. 8(a)] to single X and Z terms [shown with corresponding color in Fig. 8(b)]. Therefore, after the finite depth circuit, the two

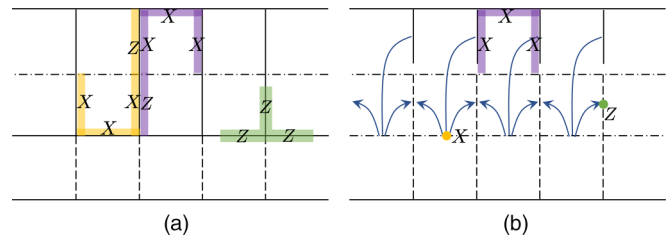

FIG. 9. Fusion of S_e [bottom in (a)] with S_ψ [top in (a)] into S_{em} [(b)] with a finite depth circuit. The circuit is composed of commuting controlled-Z gates (represented by the no-arrow connectors) and controlled-Not gates (represented by the one-arrow connectors.) Yellow and green terms map to decoupled qubits while the purple terms map to half plaquette terms on the rough boundary.

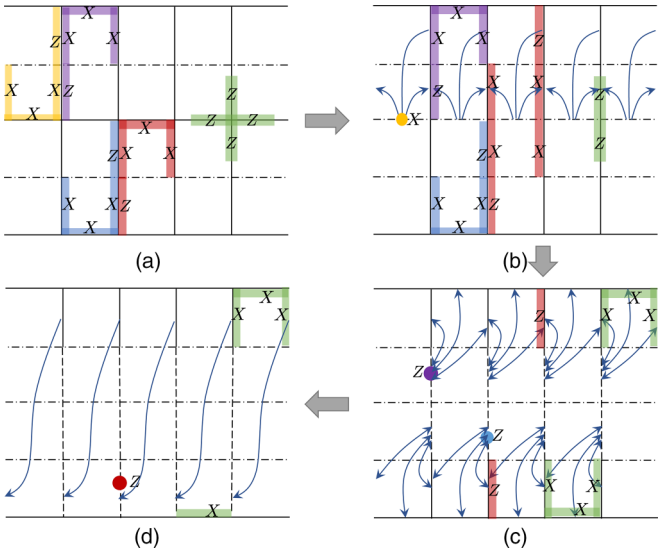

FIG. 10. Fusion of S_ψ with S_ψ into S_1 with a finite depth circuit. The circuit is composed of controlled-Z gates (the no-arrow connectors), controlled-Not gates (the one-arrow connectors) and the X-controlled-X gates (the two-arrow connectors). In (d), all qubits in the middle are decoupled while qubits on the two sides connect to form complete plaquette terms of the toric code.

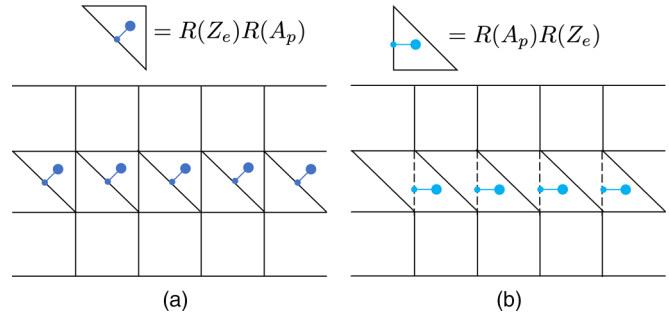

FIG. 11. Creating a dislocation in toric code with a finite depth circuit. In step 1, the dark blue gate sets are used to add diagonal edges to divide square plaquettes into triangles. In step 2, the light blue gate sets are used to remove vertical edges and merge two triangles into a parallelogram. A dislocation line is generated after these two steps.

defects merge into one, S_{em}, with smooth boundary at the bottom and rough boundary at the top.

Figure 9 shows the fusion of S_e and S_ψ into S_{em}. In Fig. 9(a), the bottom defect is the S_e defect with smooth boundaries on the two sides and the top defect is the S_ψ defect taking the form shown in Fig. 7. The circuit is composed of controlled-Z gates (represented by the no-arrow connects) and the controlled-Not gates (represented by the one-arrow connectors). All gates commute and the circuit has depth one. The yellow and green terms are mapped to single qubit terms after the circuit while the purple term becomes a three-body plaquette term on the rough side of the boundary. Therefore, S_e and S_ψ fuse into S_{em}, as shown in Fig. 9(b), which take the same form as in Fig. 8(b)

S_ψ is an invertible defect and $S_\psi \times S_\psi = S_1$. Figure 10 shows how the fusion can be realized with a finite depth circuit. The first step of the circuit [Figs. 10(a) to 10(b)] is composed of controlled-Z gates (represented by the no-arrow connects) and the controlled-Not gates (represented by the one-arrow connectors) as shown in Fig. 10(b). After this step the yellow terms map to decoupled qubits in $|+\rangle$ state on the middle line. The second step of the circuit [Figs. 10(b) to 10(c)] is composed of X-controlled-Not gates [Eq. (A3)] represented by the two-arrow connectors in Fig. 10(c). The purple and blue terms maps to decoupled qubits in this step. Finally, with controlled-Not gates in the last step [shown in Fig. 10(d) with the one-arrow connectors], the red terms map to decoupled qubits. The green terms become the plaquette term of the toric code bulk. All gates in each step of the circuit commute with each other, therefore the circuit has finite depth.

It might seem that instead of recovering the regular toric code on square lattice, we end up with a dislocation on the square lattice. But this is not a problem because a dislocation can be generated or removed with finite depth circuit in toric code as shown in Fig. 11.

Starting from a regular toric code on square lattice, diagonal edges can be added into each plaquette with the dark blue gate sets as shown in Fig. 11(a), dividing each square into two triangles. All the dark blue gate sets commute with each other and can be applied in one step. Next, the vertical edges between the triangles can be removed with the light blue gate sets as shown in Fig. 11(b), merging two triangles into a parallelogram. All light blue gate sets commute with each other as well, so we have another depth one circuit. After these two steps, we have introduced a dislocation defect into the square lattice.

[1] M. G. Alford, K. Benson, S. Coleman, J. March-Russell, and F. Wilczek, Interactions and excitations of non-abelian vortices, Phys. Rev. Lett. **64**, 1632 (1990).
[2] J. Preskill and L. M. Krauss, Local discrete symmetry and quantum-mechanical hair, Nucl. Phys. B **341**, 50 (1990).
[3] D. Gaiotto and T. Johnson-Freyd, Condensations in higher categories, arXiv:1905.09566.
[4] L. Kong, T. Lan, X.-G. Wen, Z.-H. Zhang, and H. Zheng, Classification of topological phases with finite internal symmetries in all dimensions, J. High Energy Phys. 09 (2020) 093.
[5] D. V. Else and C. Nayak, Cheshire charge in (3+1)-dimensional topological phases, Phys. Rev. B **96**, 045136 (2017).
[6] L. Kong and X.-G. Wen, Braided fusion categories, gravitational anomalies, and the mathematical framework for topological orders in any dimensions, arXiv:1405.5858.
[7] C. L. Douglas and D. J. Reutter, Fusion 2-categories and a state-sum invariant for 4-manifolds, arXiv:1812.11933.
[8] T. Lan, L. Kong, and X.-G. Wen, Classification of (3 + 1)D bosonic topological orders: The case when point-like excitations are all bosons, Phys. Rev. X **8**, 021074 (2018).
[9] L. Kong, Y. Tian, and S. Zhou, The center of monoidal 2-categories in 3+1D Dijkgraaf-witten theory, Adv. Math. **360**, 106928 (2020).

[10] T. Johnson-Freyd, On the classification of topological orders, Commun. Math. Phys. **393**, 989 (2022).
[11] L. Kong and H. Zheng, Categories of quantum liquids i, J. High Energy Phys. 08 (2022) 070.
[12] L. Kong, Y. Tian, and Z.-H. Zhang, Defects in the 3-dimensional toric code model form a braided fusion 2-category, J. High Energy Phys. 12 (2020) 078.
[13] L. Kong and H. Zheng, Categories of quantum liquids II, arXiv:2107.03858.
[14] C. Wang and M. Levin, Braiding statistics of loop excitations in three dimensions, Phys. Rev. Lett. **113**, 080403 (2014).
[15] C.-M. Jian and X.-L. Qi, Layer construction of 3D topological states and string braiding statistics, Phys. Rev. X **4**, 041043 (2014).
[16] Z. Bi, Y.-Z. You, and C. Xu, Anyon and loop braiding statistics in field theories with a topological Θ term, Phys. Rev. B **90**, 081110(R) (2014).
[17] S. Jiang, A. Mesaros, and Y. Ran, Generalized modular transformations in $(3+1)$D topologically ordered phases and triple linking invariant of loop braiding, Phys. Rev. X **4**, 031048 (2014).
[18] J. C. Wang and X.-G. Wen, Non-abelian string and particle braiding in topological order: Modular SL$(3, \mathbb{Z})$ representation and $(3+1)$-dimensional twisted gauge theory, Phys. Rev. B **91**, 035134 (2015).
[19] C. Wang and M. Levin, Topological invariants for gauge theories and symmetry-protected topological phases, Phys. Rev. B **91**, 165119 (2015).
[20] X. Chen, A. Tiwari, and S. Ryu, Bulk-boundary correspondence in (3+1)-dimensional topological phases, Phys. Rev. B **94**, 045113 (2016).
[21] M. Cheng, N. Tantivasadakarn, and C. Wang, Loop braiding statistics and interacting fermionic symmetry-protected topological phases in three dimensions, Phys. Rev. X **8**, 011054 (2018).
[22] A. Kitaev and L. Kong, Models for gapped boundaries and domain walls, Commun. Math. Phys. **313**, 351 (2012).
[23] B. Yoshida, Topological color code and symmetry-protected topological phases, Phys. Rev. B **91**, 245131 (2015).
[24] B. Yoshida, Gapped boundaries, group cohomology and fault-tolerant logical gates, Ann. Phys. (NY) **377**, 387 (2017).
[25] K. Roumpedakis, S. Seifnashri, and S.-H. Shao, Higher gauging and non-invertible condensation defects, Commun. Math. Phys. **401**, 3043 (2023).
[26] L. Kong and Z.-H. Zhang, An invitation to topological orders and category theory, arXiv:2205.05565.
[27] M. Barkeshli, Y.-A. Chen, S.-J. Huang, R. Kobayashi, N. Tantivasadakarn, and G. Zhu, Codimension-2 defects and higher symmetries in (3+1)D topological phases, SciPost Phys. **14**, 065 (2023).
[28] L. Kong, X.-G. Wen, and H. Zheng, Boundary-bulk relation in topological orders, Nucl. Phys. B **922**, 62 (2017).
[29] L. Kong, X.-G. Wen, and H. Zheng, Boundary-bulk relation for topological orders as the functor mapping higher categories to their centers, arXiv:1502.01690.
[30] C. Schön, E. Solano, F. Verstraete, J. I. Cirac, and M. M. Wolf, Sequential generation of entangled multiqubit states, Phys. Rev. Lett. **95**, 110503 (2005).
[31] C. Schön, K. Hammerer, M. M. Wolf, J. I. Cirac, and E. Solano, Sequential generation of matrix-product states in cavity qed, Phys. Rev. A **75**, 032311 (2007).
[32] M. C. Bañuls, D. Pérez-García, M. M. Wolf, F. Verstraete, and J. I. Cirac, Sequentially generated states for the study of two-dimensional systems, Phys. Rev. A **77**, 052306 (2008).
[33] Z.-Y. Wei, D. Malz, and J. I. Cirac, Sequential generation of projected entangled-pair states, Phys. Rev. Lett. **128**, 010607 (2022).
[34] X. Chen, A. Dua, M. Hermele, D. T. Stephen, N. Tantivasadakarn, R. Vanhove, and J.-Y. Zhao, Sequential quantum circuits as maps between gapped phases, Phys. Rev. B **109**, 075116 (2024).
[35] E. Dennis, A. Kitaev, A. Landahl, and J. Preskill, Topological quantum memory, J. Math. Phys. **43**, 4452 (2002).
[36] M. Aguado and G. Vidal, Entanglement renormalization and topological order, Phys. Rev. Lett. **100**, 070404 (2008).
[37] Y.-J. Liu, K. Shtengel, A. Smith, and F. Pollmann, Methods for simulating string-net states and anyons on a digital quantum computer, PRX Quantum **3**, 040315 (2022).
[38] P. Chen, B. Yan, and S. X. Cui, Quantum circuits for toric code and x-cube fracton model, Quantum **8**, 1276 (2024).
[39] Y. D. Lensky, K. Kechedzhi, I. Aleiner, and E.-A. Kim, Graph gauge theory of mobile non-abelian anyons in a qubit stabilizer code, Ann. Phys. (NY) **452**, 169286 (2023).
[40] T. I. Andersen, Y. D. Lensky, K. Kechedzhi, I. K. Drozdov, A. Bengtsson, S. Hong, A. Morvan, X. Mi, A. Opremcak, R. Acharya *et al.*, Non-abelian braiding of graph vertices in a superconducting processor, Nature (London) **618**, 264 (2023).